ENGINEERING

Crystal orientation dictated epitaxy of ultrawide-bandgap 5.4- to 8.6-eV α-$(AlGa)_2O_3$ on m-plane sapphire

Riena Jinno[1]*†, Celesta S. Chang[2,3]*, Takeyoshi Onuma[4], Yongjin Cho[1], Shao-Ting Ho[5], Derek Rowe[1], Michael C. Cao[3], Kevin Lee[1], Vladimir Protasenko[1], Darrell G. Schlom[5,6], David A. Muller[3,6], Huili G. Xing[1,5], Debdeep Jena[1,5]‡

Copyright © 2021 The Authors, some rights reserved; exclusive licensee American Association for the Advancement of Science. No claim to original U.S. Government Works. Distributed under a Creative Commons Attribution NonCommercial License 4.0 (CC BY-NC).

Ultrawide-bandgap semiconductors are ushering in the next generation of high-power electronics. The correct crystal orientation can make or break successful epitaxy of such semiconductors. Here, it is found that single-crystalline layers of α-$(AlGa)_2O_3$ alloys spanning bandgaps of 5.4 to 8.6 eV can be grown by molecular beam epitaxy. The key step is found to be the use of m-plane sapphire crystal. The phase transition of the epitaxial layers from the α- to the narrower bandgap β-phase is catalyzed by the c-plane of the crystal. Because the c-plane is orthogonal to the growth front of the m-plane surface of the crystal, the narrower bandgap pathways are eliminated, revealing a route to much wider bandgap materials with structural purity. The resulting energy bandgaps of the epitaxial layers span a broad range, heralding the successful epitaxial stabilization of the largest bandgap materials family to date.

INTRODUCTION

Since the middle of the last century, semiconductor materials have made a steady climb to the top of the periodic table to wider energy bandgaps. Starting from the early days of Ge to the Si revolution and the current wide-bandgap SiC and GaN materials, each new generation of semiconductors has enabled electronic, photonic, and sensing and actuation functions in regimes that were considered impossible before. Next-generation electronics and photonics need much larger bandgaps beyond the established material families. Ultrawide-bandgap (UWBG) semiconductor materials for power and microwave electronics and deep–ultraviolet (UV) photonics include Aluminum Nitride (AlN), Boron Nitride (BN), diamond, and Ga_2O_3 (*1*–*4*). The recent availability of single-crystal β-Ga_2O_3 substrates has generated substantial interest in this wide-bandgap semiconductor material family for high-voltage electronics and UV photonics (*5*, *6*). However, efforts to create β-$(AlGa)_2O_3$ with high Al contents to obtain UWBGs to exceed the bandgap of ~6 eV available in the nitride material family in AlN have met a roadblock. Because β-$(AlGa)_2O_3$ is not the energetically favored crystalline phase for large Al compositions, the crystal converts to competing structural phases when grown on β-Ga_2O_3 substrates (*7*–*10*).

This leads to the intriguing question: Can single-phase and highly crystalline α-Al_2O_3 of bandgap E_g ~ 8.8 eV (*11*) and its alloys and heterostructures with α-Ga_2O_3 of bandgap E_g ~ 5.3 eV (*12*–*14*) be grown directly by molecular beam epitaxy (MBE) on α-Al_2O_3 (sapphire) substrates? If this can be done, and if these layers can be controllably doped, it will open new application arenas. The UWBG energies (~5.3 to 8.8 eV), a large portion of which is unachievable in the nitride semiconductor family, and the attractive dielectric constants (~11 for || *c* axis and ~ 9 for ⊥ *c* axis for α-Al_2O_3) (*15*, *16*) offer the possibility to take semiconductor electronics and photonics into regimes that currently remain out of reach. In this work, we report that the first of these challenges can be met: High–crystalline quality, single-phase α-$(AlGa)_2O_3$ can be grown by MBE directly on m-plane sapphire, spanning bandgaps of ~5.3 to 8.8 eV, i.e., the entire Al composition of the alloy from 0 to 1. Although the conductivity control of all compositions is not achieved over the entire range of bandgaps yet, experimental evidence of n-type α-Ga_2O_3 and theoretical prediction for $(AlGa)_2O_3$ indicate that this may be feasible (*17*–*19*). The bandgaps and sharp heterostructures achieved by MBE put this material family beyond those that are available today, and the cost-effective, large-area substrates for achieving this are already available.

Significance of crystal orientation

The orientation of the substrate crystal determines the subsequent crystal phases in unique ways in this UWBG material family. Homoepitaxial growth of α-Al_2O_3 films has been reported on *c*-, *a*-, and r-plane substrates using MBE (*20*, *21*) and pulsed laser deposition (PLD) (*22*, *23*), but no study of their optical properties exist. On the other end of the α-$(Al_xGa_{1-x})_2O_3$ alloy system, single-crystalline α-Ga_2O_3 films and conductive, n-type doped films are successfully grown on *c*- and m-plane sapphire substrates by mist chemical vapor deposition (CVD) (*12*, *17*) and halide vapor-phase epitaxy (HVPE) (*24*, *25*). α-$(AlGa)_2O_3$ alloys have also been grown using MBE on a-plane ($0 \le x \le 1$) (*26*), mist-CVD on c-plane ($0 \le x \le 0.81$) (*27*–*30*), and PLD on r-plane sapphire substrates ($0.92 \le x \le 1$) (*23*). Among the growth methods, MBE and MOCVD offer the capability to maintain sharp interfaces across layers in quantum heterostructures of different alloy compositions (*8*, *21*, *31*, *32*), as well as sharply controlled doping profiles, which are problematic with HVPE or mist-CVD techniques. MBE growth of α-$(Al_xGa_{1-x})_2O_3$ of high Ga content is

[1]School of Electrical and Computer Engineering, Cornell University, Ithaca, NY 14853, USA. [2]Department of Physics, Cornell University, Ithaca, NY 14853, USA. [3]School of Applied and Engineering Physics, Cornell University, Ithaca, NY 14853, USA. [4]Department of Applied Physics, Kogakuin University, 2665-1 Hachioji, Tokyo 192-0015, Japan. [5]Department of Material Science and Engineering, Cornell University, Ithaca, NY 14853, USA. [6]Kavli Institute for Nanoscale Science, Cornell University, Ithaca, NY 14853, USA.
*These authors contributed equally to this work.
†Present address: Faculty of Pure and Applied Sciences, University of Tsukuba, Tsukuba 305-8571, Japan.
‡Corresponding author. Email: djena@cornell.edu

Downloaded from http://advances.sciencemag.org/ on January 12, 2021

hampered because metastable α-Ga_2O_3 in the rhombohedral corundum structure has a propensity to revert to the thermodynamically most stable monoclinic β-Ga_2O_3, especially whenever a corundum c-plane becomes available. This can occur either on the sapphire substrate itself or in the underlying corundum structure of the epitaxial layers. The growth of β-Ga_2O_3 on c-plane sapphire has been obtained using MOVCD and PLD (*33*), while mist-CVD and HVPE (*12*, *24*, *30*) have been used for the growth of pure α-$(AlGa)_2O_3$ on c-plane sapphire. However, as described below, the stability of the α-phase grown by MBE, MOCVD, and PLD differs significantly from those grown by mist-CVD and HVPE (*12*, *24*, *33*), which currently is a scientifically intriguing phenomena. In addition, preventing this phase transformation in MBE and MOCVD holds the key to access desired abrupt heterostructures and sharp doping profiles in this UWBG family, as indicated in Fig. 1.

The growth of β-Ga_2O_3 on c-plane sapphire substrates by MBE, MOCVD, and PLD has been found to have the epitaxial relationship of $(\bar{2}01)$ β-Ga_2O_3 || (0001) sapphire (*33*, *34*). Recent studies by scanning transmission electron microscopy (STEM) have revealed that when grown on c-plane sapphire, a three-monolayer-thick coherent α-Ga_2O_3 first forms, and the subsequent epitaxial layers undergo a crystalline phase transition to the β-phase (*33*), as shown in Fig. 1A. Also shown in the figure are the planes $(\bar{2}01)$ β-Ga_2O_3 || (0001) sapphire, which cause this transition. As shown in Fig. 1A, if the hexagonal sapphire crystal plane is rotated from the c-plane to the r-plane, the c-plane is now at an angle and can potentially stabilize the growth of α-Ga_2O_3 by avoiding the crystalline phase transition.

In 2018, Kracht *et al.* attempted this strategy: They reported the growth of α-Ga_2O_3 on r-plane sapphire substrate with a film thickness of 217 nm (*14*). They observed that after c-plane facets were formed on the surface of the α-Ga_2O_3 film, the β-Ga_2O_3 appeared with the same epitaxial relationship of $(\bar{2}01)$ β-Ga_2O_3 || (0001) α-Ga_2O_3/sapphire, as shown in Fig. 1B, indicating that the c-plane facet enhanced the growth of β-Ga_2O_3 in MBE. These results suggest that a sapphire crystal plane perpendicular to the c-plane, such as a- or m-planes, could potentially allow the growth of phase-pure α-Ga_2O_3 by avoiding facets, as shown in Fig. 1C. Nd-doped α-$(Al_xGa_{1-x})_2O_3$ and α-Ga_2O_3 with a film thickness of 14 nm have been reported on a-plane sapphire in previous studies (*26*, *34*). These prior studies provided x-ray diffraction (XRD) study of the layers, but the atomic crystal structure and optical properties remain unknown.

The MBE growth of α-$(Al_xGa_{1-x})_2O_3$ material family on m-plane sapphire has not been investigated in detail. However, Sn-doped α-Ga_2O_3 of bandgap ~5.3 eV on m-plane sapphire grown by mist-CVD exhibits a room temperature electron mobility of 65 $cm^2/V{\cdot}s$ at a high carrier density of $n = 1.2 \times 10^{18}$ cm^{-3} (*18*), suggesting promising electronic properties of α-$(Al_xGa_{1-x})_2O_3$ on m-plane sapphire. High room temperature electron mobility of ~600 $cm^2/V{\cdot}s$ was concluded for optically generated electrons in α-Al_2O_3, increasing to ~4000 $cm^2/V{\cdot}s$ at low temperatures (*35*). A recent first-principles study predicts that Si can be an efficient shallow donor for high–Al content $(Al_xGa_{1-x})_2O_3$ (*19*), to achieve n-type conductivity of $(Al_xGa_{1-x})_2O_3$.

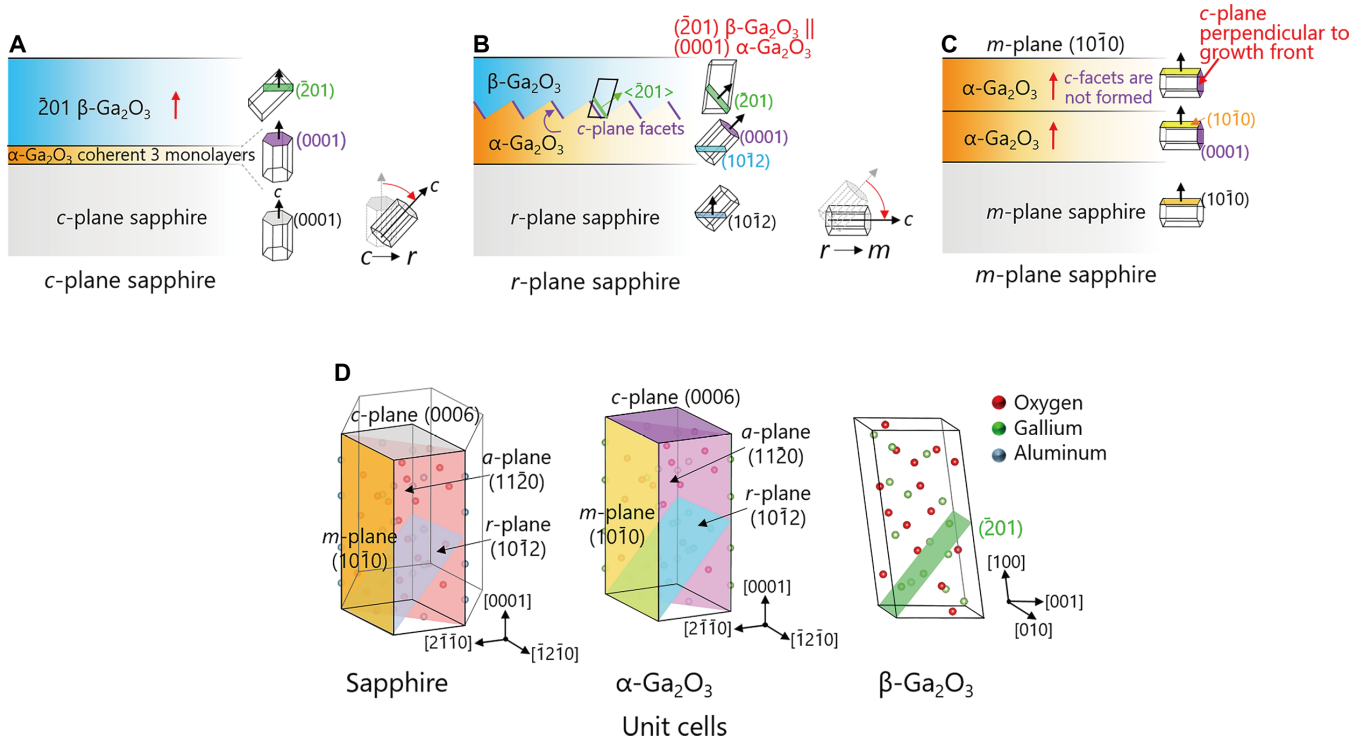

Fig. 1. Schematics of growth behaviors of Ga_2O_3 grown on sapphire. Schematics of growth behaviors of Ga_2O_3 grown on (**A**) c-plane, (**B**) r-plane, and (**C**) m-plane sapphire substrates by MBE and (**D**) unit cells of sapphire, α-Ga_2O_3, and β-Ga_2O_3. β-Ga_2O_3 is grown on c-plane sapphire substrates with the coherent α-Ga_2O_3 interlayer. (*33*) The epitaxial relationship is $(\bar{2}01)$ β-Ga_2O_3 || (0001) α-Ga_2O_3/sapphire. On r-plane sapphire, after c-plane facets are formed on the surface of the α-Ga_2O_3 layer, β-Ga_2O_3 appears with the same epitaxial relationship of $(\bar{2}01)$ β-Ga_2O_3 || (0001) α-Ga_2O_3 (*14*). On the other hand, m-plane, which is perpendicular to the c-plane, is expected to have less chance to form the c-plane facets and allow the growth of phase-pure α-Ga_2O_3.

Downloaded from http://advances.sciencemag.org/ on January 12, 2021

Motivated by the above reasons, in this study, we explore growth of this UWBG semiconductor family on m-plane sapphire substrates. We find that the MBE growth of α-$(Al_xGa_{1-x})_2O_3$ on m-plane sapphire solves the faceting problem completely, allowing its bandgap engineering over the entire composition range to be achieved. A series of epitaxial layers of α-$(Al_xGa_{1-x})_2O_3$ with $x = 0.0$ to 1.0 and thicknesses ranging from ~50 to 85 nm were grown by oxygen plasma-assisted MBE on m-plane sapphire substrates. The growth and subsequent structural, chemical, and optical characterization methods are described in Materials and Methods.

RESULTS AND DISCUSSION

Single-crystal UWBG epitaxial layers

Symmetric XRD 2θ/ω scans of the samples are displayed in a logarithmic intensity scale in Fig. 2A. The profiles reveal that the diffraction peak is from the α-$(Al_xGa_{1-x})_2O_3$ $30\bar{3}0$ reflection at angles slightly lower than that of the sapphire substrate. There are no peaks originating from other crystal phases or other planes. With decreasing Al composition x, the peaks from α-$(Al_xGa_{1-x})_2O_3$ $30\bar{3}0$ monotonically shift to lower angles without any compositional segregation, suggesting a higher Ga composition in the film. No additional peaks or fringes are observed for the MBE-grown α-Al_2O_3 epitaxial layer, which is identical to the substrate despite the ~60-nm thickness, as verified by secondary ion mass spectrometry (SIMS) discussed later. From these results, we conclude that single-phase α-$(Al_xGa_{1-x})_2O_3$ films are epitaxially stabilized successfully on m-plane sapphire substrates for the entire range of Al compositions without phase or composition separation/segregation.

Figure 2B shows the SIMS profiles measured on the homoepitaxial 100% α-Al_2O_3 layer grown on m-plane sapphire. The atomic concentrations of typical impurities (H, B, C, Na, and Si) are indicated by the axis on the left, while secondary intensities of Al and O are shown on the axis on the right. The intensities of Al and O in the epitaxial layer are observed to be identical to that in the m-plane sapphire substrate, suggesting growth of stoichiometric Al_2O_3. Compared to the sapphire substrate, a large B peak is seen at the growth interface, which is a marker indicating that the film thickness of the MBE-grown α-Al_2O_3 epitaxial layer is ~60 nm. There is an increase in the Si concentration at the growth interface, whereas the H and C concentrations in the epitaxial layer remain identical to the m-plane sapphire bulk substrate. The profiles for H and C represent the background levels of the measurements since densities of ~10^{18} cm^{-3} are not expected in sapphire substrates. The Na concentration is ~10^{16} cm^{-3}. At present, we assume that the source of B is the pBN crucibles used for the MBE source materials, that of Si is from the quartz tube used as a component of the O plasma source, and that of Na is from the sapphire substrate. Si could accumulate during the substrate treatment using O plasma before growth as discussed in Materials and Methods.

To evaluate the strain in the epitaxial films, asymmetrical reciprocal space maps (RSMs) for $22\bar{4}0$ reflections were taken. Figure 3A shows the relation between the $(22\bar{4}0)$ and $(10\bar{1}0)$ m-plane of the corundum structure. These results indicate that the α-$(Al_xGa_{1-x})_2O_3$ films ($0.37 \leqq x \leqq 0.74$) consist of coherent and relaxed layers, and the relaxed layers are subject to slight in-plane compressive strain (Fig. 3, C to F). On the other hand, the α-$(Al_xGa_{1-x})_2O_3$ films ($x < 0.37$) were completely lattice-relaxed because of the lattice mismatch with the sapphire substrate (fig. S1). Because $22\bar{4}0$ decomposes into $30\bar{3}0$ + $\bar{1}2\bar{1}0$, the directions of Q_z and Q_x are along $10\bar{1}0$ (the growth direction) and $\bar{1}2\bar{1}0$ (one of the a axes), respectively. The dashed red line intersects the theoretical positions of sapphire [$(Q_x, Q_z) = (-0.420, 0.728)$] and α-$Ga_2O_3$ $22\bar{4}0$ reflection [$(Q_x, Q_z) = (-0.401, 0.695)$]. The α-$Al_2O_3$ homoepitaxial film shows a streak along $Q_x = -0.42$ $Å^{-1}$ (Fig. 3B), which is also observed for the reflections at $Q_x = -0.42$ $Å^{-1}$ in the samples whose x is larger than 0.37. The vertical streak arises from a small film thickness. Two reflection peaks of α-$(Al_xGa_{1-x})_2O_3$ are obtained at x between 0.37 and 0.74: One is on the same Q_x line ($Q_x = -0.42$) as that of the sapphire substrate and the other is located between the dashed line and $Q_x = -0.42$ $Å^{-1}$ (Fig. 3, C to F).

Figure 4 shows the surface atomic force microscopy (AFM) images of the m-plane sapphire substrate and the epitaxial α-$(Al_xGa_{1-x})_2O_3$ films. The surface morphology of the as-received

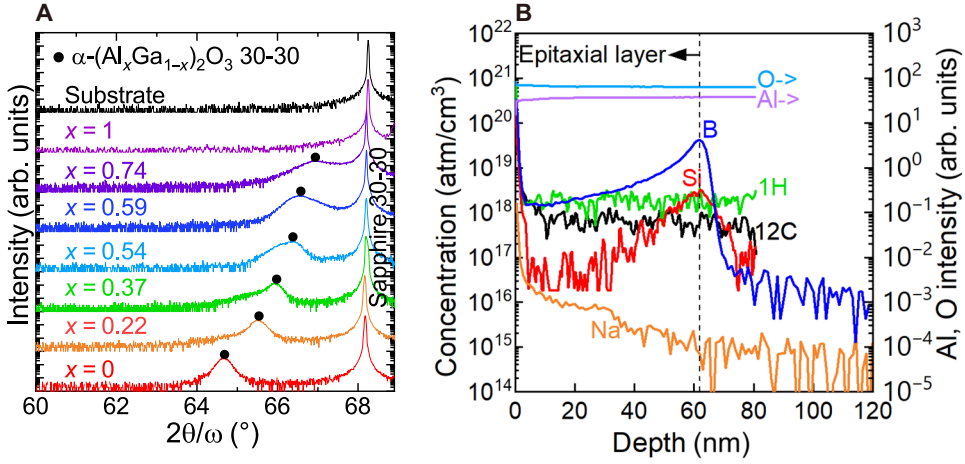

Fig. 2. XRD scans of α-$(Al_xGa_{1-x})_2O_3$ films and SIMS profiles of the α-Al_2O_3 epitaxial film. (**A**) Symmetric XRD 2θ/ω scans of α-$(Al_xGa_{1-x})_2O_3$ films grown on m-plane sapphire substrates by plasma-assisted MBE. Diffraction peaks from the α-$(Al_xGa_{1-x})_2O_3$ are denoted by the filled circles. Note that no diffraction peaks from other phases are observed. (**B**) Atomic densities of typical impurities in the α-Al_2O_3 epitaxial film grown on m-plane sapphire measured by SIMS. The film/substrate interface is marked by the clear peak in the B profile, indicating that the epitaxial film thickness is ~60 nm. The concentrations of H and C are at background levels. Secondary ion intensities of Al and O are also shown on the side axis on the right, indicating stoichiometric epitaxial growth.

Downloaded from http://advances.sciencemag.org/ on January 12, 2021

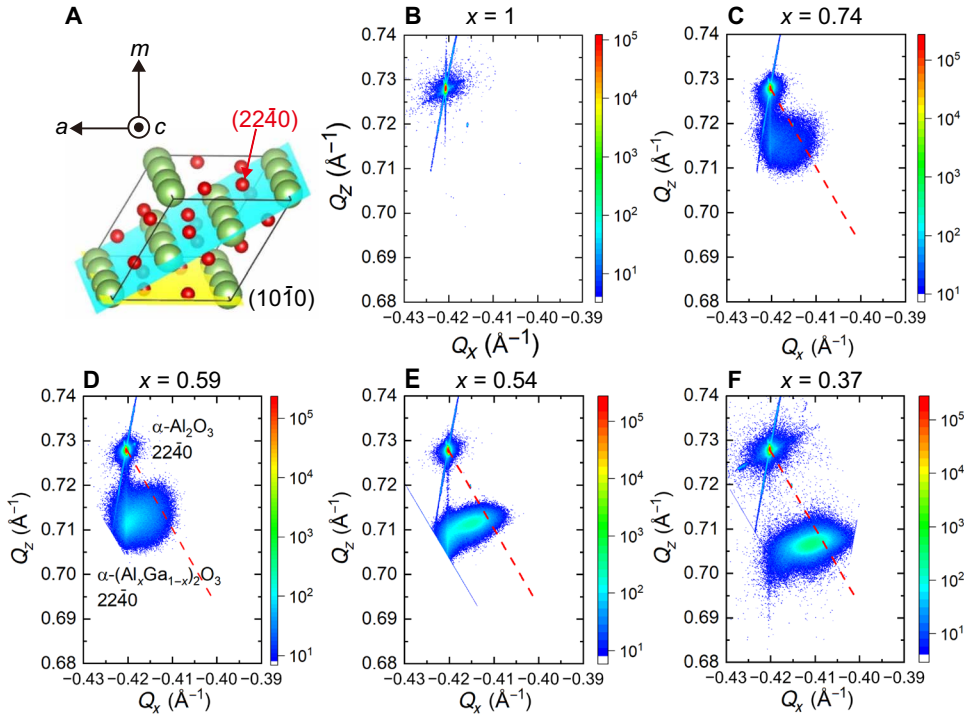

Fig. 3. RSMs (Q_x, Q_z) around the 22$\bar{4}$0 reflections of the α-$(Al_xGa_{1-x})_2O_3$ epitaxial films. (**A**) The relation between the (22$\bar{4}$0) and (10$\bar{1}$0) *m*-plane of the corundum structure. The directions of Q_z and Q_x are along 10$\bar{1}$0 and $\bar{1}$2$\bar{1}$0, respectively. RSMs for x = (**B**) 0, (**C**) 0.74, (**D**) 0.59, (**E**) 0.54, and (**F**) 0.37.

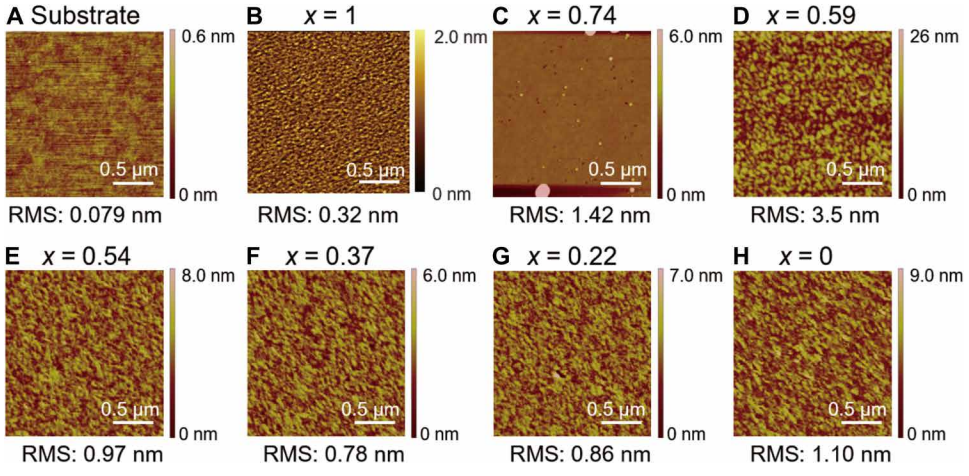

Fig. 4. Surface morphology of α-$(Al_xGa_{1-x})_2O_3$ films on *m*-plane sapphire substrates. (**A**) Sapphire substrate. (**B**) to (**H**) are α-$(Al_xGa_{1-x})_2O_3$ films with x = 1, 0.74, 0.59, 0.54, 0.37, 0.22, and 0, respectively. The RMS roughness of the α-$(Al_xGa_{1-x})_2O_3$ films for $x \leq 0.54$ is less than 1.1 nm.

substrate was extremely smooth with a root mean square (RMS) roughness as small as 0.079 nm (Fig. 4A). The α-Al_2O_3 epitaxial film shows a small RMS roughness of 0.32 nm (Fig. 4B) but does not exhibit atomic steps, which are not observed on the starting substrate either. Curiotto *et al.* reported a step-terrace morphology for *m*-plane sapphire substrates by annealing under Ar-O_2 at 1235 K for 78 hours (*36*), suggesting thermal treatment for potential improvement of the surface morphology of α-Al_2O_3 films in the future. When the Al mole fraction x is smaller than 0.54, the RMS roughness remains smaller than 1.1 nm (Fig. 4, E to H). For x = 0.59 and x = 0.74, α-$(Al_xGa_{1-x})_2O_3$ films have rougher surface morphologies of 3.5 and 1.42 nm RMS values (Fig. 4, C and D), probably due to the low substrate temperature of 650°C.

Electron microscopy reveals single-crystalline UWBG layers

The XRD spectra showed the growth of single-phase α-$(Al_xGa_{1-x})_2O_3$ films on m-plane sapphire substrates. To investigate the atomic details of the crystal structures of the epitaxial layers, high-angle annular dark-field STEM (HAADF-STEM) images were taken on the cross-sectional α-$(Al_xGa_{1-x})_2O_3$ samples for x = 1, x = 0.37, x = 0.22,

Downloaded from http://advances.sciencemag.org/ on January 12, 2021

and $x = 0$. All the images were viewed along the ⟨0001⟩ zone axis. Figure 5 shows the cross-sectional images of the α-$(Al_xGa_{1-x})_2O_3$ film series grown on m-plane sapphire substrates and the corresponding enlarged images at the interfaces. As shown in Fig. 5A, since the epitaxial α-Al_2O_3 layer and the substrate have the same contrast, the exact location of the interface is invisible. On the basis of the corroborating SIMS measurement of Fig. 2B, an enlarged image was taken at the interface that was formed 60 nm below the surface. The uniformity of the crystal structure indicates that epitaxial α-Al_2O_3 films grow homoepitaxially on m-plane sapphire substrate with no visible structural defects.

On the other hand, a clear contrast between the epitaxial film and the substrate is seen for the images of the α-$(Al_{0.37}Ga_{0.63})_2O_3$, α-$(Al_{0.22}Ga_{0.78})_2O_3$, and α-$Ga_2O_3$ samples (Fig. 5, B to D). The low-magnification images reveal that these films grow uniformly on m-plane sapphire substrates. Contrast variations inside the film are due to strain relaxation by misfit dislocations near the substrate interface. The edge dislocation density is estimated at ~5×10^5 cm^{-1} (or ~10^{11} cm^{-2}) from the cross-sectional TEM sample of α-$(Al_{0.37}Ga_{0.63})_2O_3$, in the range also corroborated by x-ray rocking curves as shown in fig. S2 and table S2 discussed in the Supplementary Materials. This is consistent with the incoherent nature of the α-$(Al_{0.37}Ga_{0.63})_2O_3$ epitaxial layer indicated by RSM of Fig. 3F compared to the coherent α-Al_2O_3 epitaxial layer in Fig. 3B. No notable phase separation or compositional segregation is observed in the epitaxial layers: They are phase pure. The film thicknesses of the α-$(Al_{0.37}Ga_{0.63})_2O_3$, α-$(Al_{0.22}Ga_{0.78})_2O_3$, and α-$Ga_2O_3$ films are measured to be 66, 57, and 60 nm, respectively, which agree well with the thicknesses (d) estimated from x-ray reflectivity (XRR) measurements (table S1). The enlarged images show that sharp heterojunction interfaces are formed between the epitaxial films and the substrates and that the α-$(Al_xGa_{1-x})_2O_3$ ($x \leq 0.37$) films have an identical crystal structure and orientation to the substrate. α-Ga_2O_3 films show dislocations at the interface due to lattice mismatch (Fig. 5D and fig. S3); however, no secondary phases were observed. The combination of the STEM images with XRD thus indicates that single-crystalline, single-phase epitaxial films are successfully grown on the m-plane sapphire substrate over the full $0 \leq x \leq 1$ composition range.

Deep-UV spectroscopy reveals UWBGs

Figure 6A shows the optical transmittance spectra of the α-$(Al_xGa_{1-x})_2O_3$ films (T) and a bare m-plane sapphire substrate control sample (T_s) as a function of the photon energy ($h\nu$). Each epitaxial film shows the same high transparency in the visible and UV spectral ranges as the substrate. The bandgaps of the epitaxial α-$(Al_xGa_{1-x})_2O_3$ layers are clearly observed despite their small thicknesses, indicating strong photon absorption. Note that the transmittance of

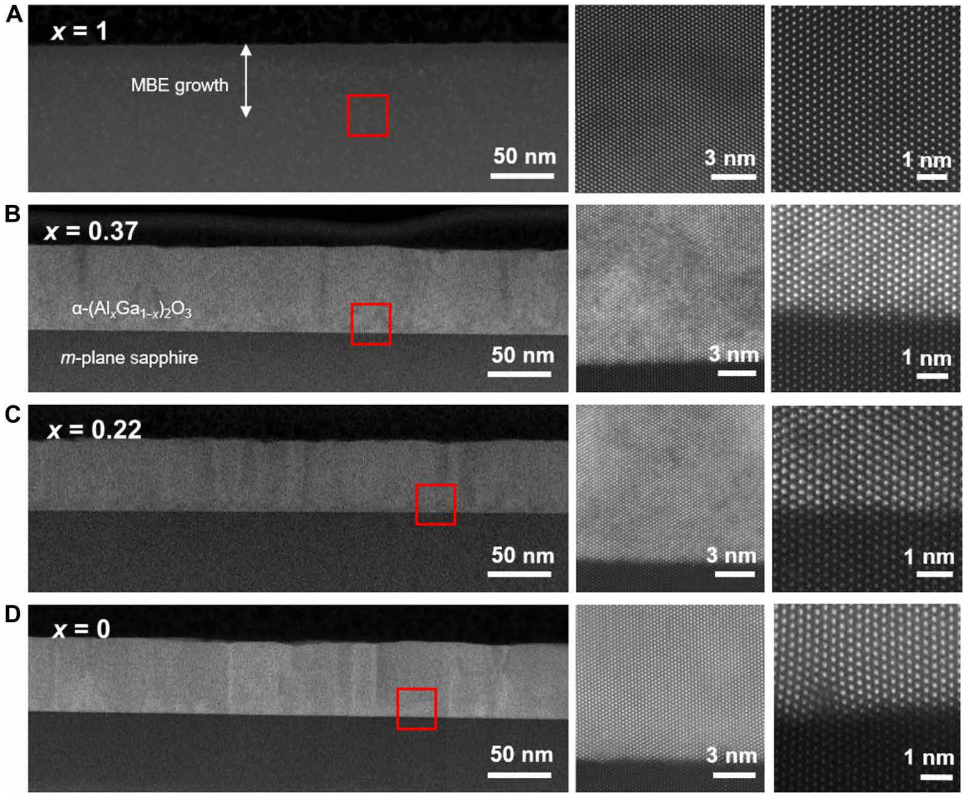

Fig. 5. HAADF-STEM images showing an overview of α-$(Al_xGa_{1-x})_2O_3$ film grown on m-plane sapphire and the sequentially enlarged interfaces from the boxes in the overview images. (A) to (D) correspond to $x = 1$, $x = 0.37$, $x = 0.22$, and $x = 0$, respectively. (**A**) The film and the substrate show identical contrast, as expected for a homoepitaxial film. The enlarged area shows no differences in contrast and lattice structure. (**B**) to (**D**) show film thickness of 66, 55, and 60 nm, respectively. They all show sharp interfaces, while the films show contrast variations from strain relaxation resulting from misfit dislocations near the interface. Further details of the defects are explained in the Supplementary Materials. Enlarged atomic resolution image in (D) shows that α-Ga_2O_3 film is relaxed at the interface; however, no other phases are observed.

Downloaded from http://advances.sciencemag.org/ on January 12, 2021

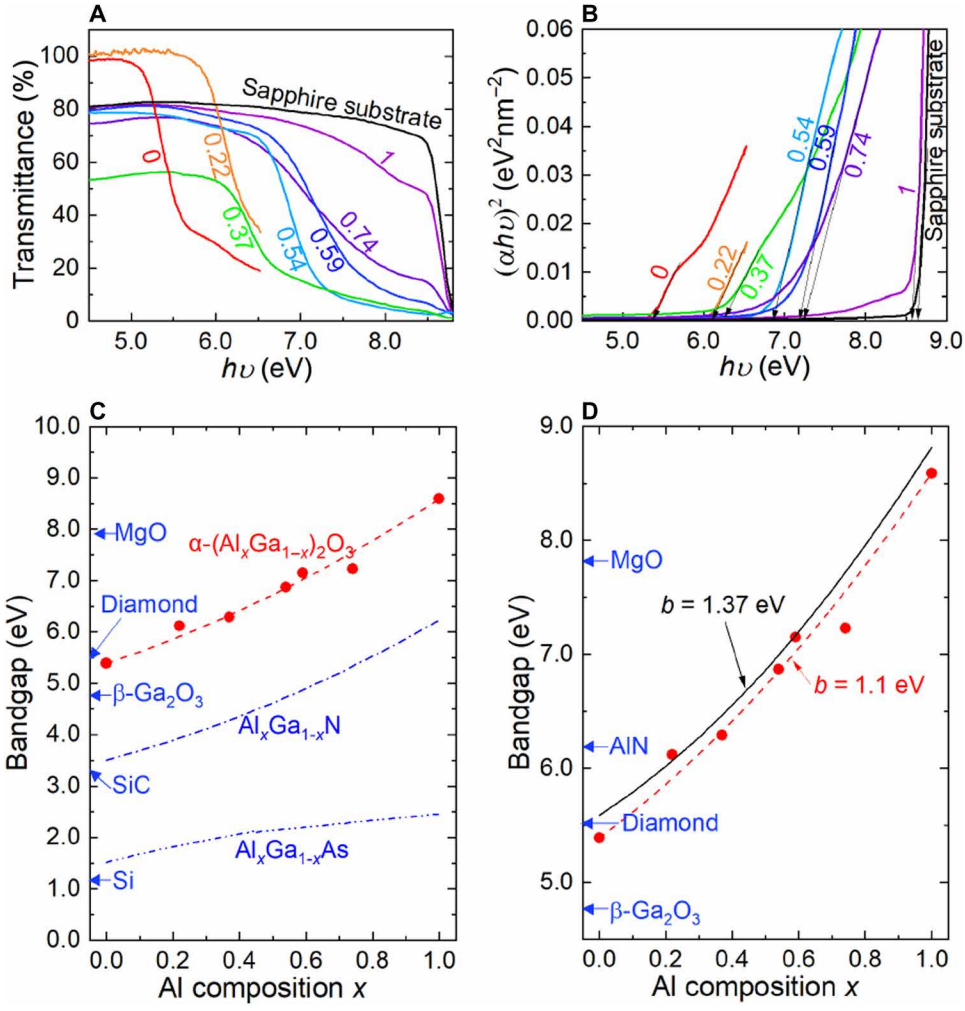

Fig. 6. Optical transmittance spectra and bandgap energies of the α-$(Al_xGa_{1-x})_2O_3$ films. (**A**) Optical transmittance of the α-$(Al_xGa_{1-x})_2O_3$ films and substrate. (**B**) $(\alpha h\nu)^2$-$h\nu$ plot as a function of the Al composition. The α-$(Al_{0.37}Ga_{0.63})_2O_3$ film exhibited a lower transmittance than the other samples since the sample was smaller than the aperture for the transmittance measurement. The appearance of higher transparency of the samples with $x = 0$ and $x = 0.22$ is due to different measurement systems. Compared to the absorption spectra of the bulk α-Al_2O_3 substrate, the transmittance and absorption spectra of the α-Al_2O_3 epitaxial sample shows absorption around 7 to 8.5 eV and what appears as a slight red shift in the fundamental absorption edge. Both are attributed to absorption by sub-bandgap defect states (likely O and/or Al interstitials or vacancies) since the TEM image in Fig. 5A does not show extended defects, nor does the SIMS profile (Fig. 2B). Direct bandgaps (solid symbols) for the α-$(Al_xGa_{1-x})_2O_3$ films as a function of the Al composition are shown in (**C**) the wide range from 0 to 10 eV and (**D**) the UWBG region ($E_g > 4$ eV). The red dashed line is a quadratic fit to the direct bandgaps. The black solid line is a quadratic fit to the computed direct bandgap for the corundum structure as reported in (*37*). The bandgaps for AlGaN and AlGaAs are also shown for comparison in (C) (*38*).

α-$(Al_{0.37}Ga_{0.63})_2O_3$ appears lower than the other samples because of a smaller sample size of this particular sample than the optical aperture. Each absorption coefficient (α) was calculated using the equation $T/T_s = \exp(-\alpha d)$, and $(\alpha h\nu)^2$ is plotted as a function of $h\nu$ in Fig. 6B. When $x = 0$ and 0.22, the absorption edge exhibits a double step-like onset, while the α-$(Al_xGa_{1-x})_2O_3$ ($x \geq 0.37$) has a single step onset. The observation of double step-like onset in α-Ga_2O_3 thin films has been reported earlier, suggesting two allowed direct optical interband transitions (*13*, *14*). The Ga-rich α-$(Al_xGa_{1-x})_2O_3$ films ($0 \leq x \leq 0.37$) show broader absorption onsets than the Al-rich samples, which is related to the slightly indirect bandgap character of α-Ga_2O_3 (*13*).

Direct optical bandgap energies of the α-$(Al_xGa_{1-x})_2O_3$ films were estimated from the relationship of $(\alpha h\nu)^2$ versus ($h\nu$-E_g). As shown by the red filled circles in Fig. 6C, the experimental direct bandgaps monotonically increase as the Al composition x increases. In Fig. 6D, the black solid line shows the theoretical direct bandgap energies calculated by Peelaers *et al.* (*37*) using hybrid density functional theory. The experimentally measured bandgaps of the α-$(Al_xGa_{1-x})_2O_3$ epitaxial layers are, for the most part, in excellent agreement. A ~0.2 eV lower than the predicted values from the simple Tauc plots of $(\alpha h\nu)^2$ versus ($h\nu$-E_g) may be due to an underestimation of the bandgap energy owing to excitonic absorption with low-energy tails, related to the slightly indirect character of α-Ga_2O_3 and to as-yet unknown defects (*13*). The bowing parameter (b) is obtained from $E_g(x) = (1 - x)E_g[Ga_2O_3] + xE_g[Al_2O_3] - bx(1 - x)$, where $E_g[Ga_2O_3]$ and $E_g[Al_2O_3]$ are the bandgap energies of α-Ga_2O_3 and α-Al_2O_3, respectively, by fitting the plot as depicted by the red

Downloaded from http://advances.sciencemag.org/ on January 12, 2021

dashed line. The value of b is estimated to be 1.1 eV. This experimental value agrees well with the theoretically calculated value of 1.37 eV and proves the UWBG nature of the epitaxial layers available for bandgap engineering from 5.4 to 8.6 eV.

In conclusion, we have demonstrated the successful epitaxial stabilization of UWBG single-phase α-$(Al_xGa_{1-x})_2O_3$ films over the entire composition range on m-plane sapphire substrates by MBE by avoiding phase transformation with the choice of crystal orientation for epitaxy. Cross-sectional HAADF-STEM images reveal that single-phase, single-crystalline α-$(Al_xGa_{1-x})_2O_3$ epitaxial films are formed, by avoiding the formation of c-plane facets. By varying the alloy composition, bandgap energies from ~5.4 eV up to 8.6 eV with a bowing parameter of 1.1 eV are achieved, making α-$(Al_xGa_{1-x})_2O_3$ the largest bandgap epitaxial material family to date. If these layers can be controllably doped, it would pave the way for α-$(Al_xGa_{1-x})_2O_3$–based high-power heterostructure electronic and photonic devices at bandgaps far beyond all materials available today.

MATERIALS AND METHODS

Materials

All films reported in this work were grown on double-side polished m-plane $(10\bar{1}0)$ sapphire substrates in the Veeco Gen930 MBE System equipped with standard effusion cells for elemental Ga and Al and a radio frequency (RF) plasma source for active oxygen species. The pressure in the growth chamber was ~10^{-5} to 10^{-6} torr during the growth runs. For the growth of α-$(Al_xGa_{1-x})_2O_3$ films ($x \geq 0.37$), the input RF power and oxygen flow rate were fixed at 250 W and 0.50 sccm (standard cubic centimeters per minute), respectively. The α-Al_2O_3 and α-$(Al_xGa_{1-x})_2O_3$ films ($1 > x \geq 0.37$) were grown for 2 hours at thermocouple substrate temperatures (T_{sub}) of 750°C and 650°C, respectively. The α-$(Al_xGa_{1-x})_2O_3$ ($x = 0.22$ and 0) samples were grown at T_{sub} = 650°C using the input RF power of 260 W and the oxygen flow rate of 0.23 sccm. The growth times of α-$(Al_{0.22}Ga_{0.78})_2O_3$ and α-Ga_2O_3 were 3 hours and 3 hours 13 min, respectively. The Al concentration (x) in the films was varied from 0 to 1 by regulating the beam equivalent pressures (BEPs) of Ga [(0 to 1.1) × 10^{-8} torr] and Al [(0 to 1.6) × 10^{-8} torr]. Before each growth, the m-plane sapphire substrates were subjected to an oxygen plasma treatment in the growth chamber for 10 min at T_{sub} = 800°C.

Characterization of materials

Structural properties and surface morphology of the samples were characterized by XRD measurements, AFM, and STEM. The film thicknesses of the samples ($x < 1$) were determined by XRR measurements, while SIMS was used to determine the chemical impurity species as well as the thickness of the α-Al_2O_3 epitaxial layer, since there were no thickness fringes observed from the XRR profile for the α-Al_2O_3 film due to homoepitaxial growth. The film thicknesses were in the range of 56 to 84.3 nm. Table S1 summarizes the Al and Ga BEPs and film thicknesses (d) of the samples. The Al composition was estimated by XRD and x-ray photoelectron spectroscopy (XPS). Optical bandgaps of the films were estimated by analyzing the optical transmission spectra; an m-plane sapphire substrate was used as a reference sample. The optical transmittance spectra were measured at room temperature using a Varian Cary 50 UV-Vis spectrometer with a wavelength range of 190 to 800 nm for $x \leq 0.22$ and using a Bunkoukeiki KV-201 vacuum UV spectrophotometer with a wavelength range of 140 to 300 nm for $x \geq 0.37$. The Bunkoukeiki KV-201 unit had a 20-cm focal-length Czerny-Turner monochromator equipped with a 1200 groove/mm grating and a 30-W deuterium lamp that were purged with nitrogen gas during operation. A separate α-Al_2O_3 sample used for transmittance measurement was grown at T_{sub} = 750°C for 2 hours using an input RF power of 250 W, an oxygen flow rate of 0.50 sccm, and an Al BEP of 1.5 × 10^{-8} torr. By inserting a thin α-Ga_2O_3 layer to intentionally introduce thickness fringes, the film thickness of 78.2 nm was measured by XRR. We used the sample directly grown on sapphire in the same growth condition for the transmittance measurement.

Transmission electron microscopy measurement

Cross-sectional TEM specimens were prepared using a FEI Strata 400 Focused Ion Beam with a final milling step of 5 keV to reduce damage. Carbon and platinum protective layers were deposited before milling to minimize ion-beam damage. The samples were then examined by STEM, using an aberration-corrected Titan Themis operating at 300 keV.

SUPPLEMENTARY MATERIALS

Supplementary material for this article is available at http://advances.sciencemag.org/cgi/content/full/7/2/eabd5891/DC1

REFERENCES AND NOTES

1. A. M. Armstrong, M. W. Moseley, A. A. Allerman, M. H. Crawford, J. J. Wierer, Growth temperature dependence of Si doping efficiency and compensating deep level defect incorporation in $Al_{0.7}Ga_{0.3}N$. *J. Appl. Phys.* **117**, 185704 (2015).
2. R. J. Kaplar, A. A. Allerman, A. M. Armstrong, M. H. Crawford, J. R. Dickerson, A. J. Fischer, A. G. Baca, E. A. Douglas, Review—Ultra-wide-bandgap AlGaN power electronic devices. *ECS J. Solid State Sci. Technol.* **6**, Q3061–Q3066 (2017).
3. S. Fujita, M. Oda, K. Kaneko, T. Hitora, Evolution of corundum-structured III-oxide semiconductors: Growth, properties, and devices. *Jpn. J. Appl. Phys.* **55**, 1202A3 (2016).
4. J. Y. Tsao, S. Chowdhury, M. A. Hollis, D. Jena, N. M. Johnson, K. A. Jones, R. J. Kaplar, S. Rajan, C. G. Van de Walle, E. Bellotti, C. L. Chua, R. Collazo, M. E. Coltrin, J. A. Cooper, K. R. Evans, S. Graham, T. A. Grotjohn, E. R. Heller, M. Higashiwaki, M. S. Islam, P. W. Juodawlkis, M. A. Khan, A. D. Koehler, J. H. Leach, U. K. Mishra, R. J. Nemanich, R. C. N. Pilawa-Podgurski, J. B. Shealy, Z. Sitar, M. J. Tadjer, A. F. Witulski, M. Wraback, J. A. Simmons, Ultrawide-bandgap semiconductors: Research opportunities and challenges. *Adv. Electron. Mater.* **4**, 1600501 (2018).
5. M. Higashiwaki, K. Sasaki, A. Kuramata, T. Masui, S. Yamakoshi, Gallium oxide (Ga_2O_3) metal-semiconductor field-effect transistors on single-crystal β-Ga_2O_3 (010) substrates. *Appl. Phys. Lett.* **100**, 013504 (2012).
6. W. Li, K. Nomoto, Z. Hu, T. Nakamura, D. Jena, H. G. Xing, in *2019 IEEE International Electron Devices Meeting (IEDM)* (IEEE, 2019), pp. 12.4.1–12.4.4; https://ieeexplore.ieee.org/document/8993526/.
7. T. Oshima, T. Okuno, N. Arai, Y. Kobayashi, S. Fujita, β-$Al_{2x}Ga_{2-2x}O_3$ thin film growth by molecular beam epitaxy. *Jpn. J. Appl. Phys.* **48**, 070202 (2009).
8. S. W. Kaun, F. Wu, J. S. Speck, β-$(Al_xGa_{1-x})_2O_3/Ga_2O_3$ (010) heterostructures grown on β-Ga_2O_3 (010) substrates by plasma-assisted molecular beam epitaxy. *J. Vac. Sci. Technol.* **33**, 041508 (2015).
9. A. F. M. Anhar Uddin Bhuiyan, Z. Feng, J. M. Johnson, Z. Chen, H.-L. Huang, J. Hwang, H. Zhao, MOCVD epitaxy of β-$(Al_xGa_{1-x})_2O_3$ thin films on (010) Ga_2O_3 substrates and N-type doping. *Appl. Phys. Lett.* **115**, 120602 (2019).
10. A. F. M. A. U. Bhuiyan, Z. Feng, J. M. Johnson, H.-L. Huang, J. Sarker, M. Zhu, M. R. Karim, B. Mazumder, J. Hwang, H. Zhao, Phase transformation in MOCVD growth of $(Al_xGa_{1-x})_2O_3$ thin films. *APL Mater.* **8**, 031104 (2020).
11. R. H. French, Electronic band structure of Al_2O_3, with comparison to Alon and AlN. *J. Am. Ceram. Soc.* **73**, 477–489 (1990).
12. D. Shinohara, S. Fujita, Heteroepitaxy of corundum-structured α-Ga_2O_3 thin films on α-Al_2O_3 substrates by ultrasonic mist chemical vapor deposition. *Jpn. J. Appl. Phys.* **47**, 7311–7313 (2008).
13. A. Segura, L. Artús, R. Cuscó, R. Goldhahn, M. Feneberg, Band gap of corundumlike α–Ga_2O_3 determined by absorption and ellipsometry. *Phys. Rev. Mater.* **1**, 024604 (2017).
14. M. Kracht, A. Karg, M. Feneberg, J. Bläsing, J. Schörmann, R. Goldhahn, M. Eickhoff, Anisotropic optical properties of metastable $(01\bar{1}2)$ α-Ga_2O_3 grown by plasma-assited molecular beam epitaxy. *Phys. Rev. Appl.* **10**, 024047 (2018).

Downloaded from http://advances.sciencemag.org/ on January 12, 2021

15. A. K. Harman, S. Ninomiya, S. Adachi, Optical constants of sapphire (α-Al_2O_3) single crystals. *J. Appl. Phys.* **76**, 8032–8036 (1994).
16. J. Fontanella, C. Andeen, D. Schuele, Low-frequency dielectric constants of α-quartz, sapphire, MgF_2, and MgO. *J. Appl. Phys.* **45**, 2852–2854 (1974).
17. K. Akaiwa, S. Fujita, Electrical conductive corundum-structured α-Ga_2O_3 thin films on sapphire with tin-doping grown by spray-assisted mist chemical vapor deposition. *Jpn. J. Appl. Phys.* **51**, 070203 (2012).
18. K. Akaiwa, K. Ota, T. Sekiyama, T. Abe, T. Shinohe, K. Ichino, Electrical properties of Sn-doped α-Ga_2O_3 films on m-plane sapphire substrates grown by mist chemical vapor deposition. *Phys. status solidi.* **217**, 1900632 (2020).
19. J. B. Varley, A. Perron, V. Lordi, D. Wickramaratne, J. L. Lyons, Prospects for n-type doping of $(Al_xGa_{1-x})_2O_3$ alloys. *Appl. Phys. Lett.* **116**, 172104 (2020).
20. T. Maeda, M. Yoshimoto, T. Ohnishi, G. H. Lee, H. Koinuma, Orientation-defined molecular layer epitaxy of α-Al_2O_3 thin films. *J. Cryst. Growth* **177**, 95–101 (1997).
21. T. Oshima, Y. Kato, M. Imura, Y. Nakayama, M. Takeguchi, α-Al_2O_3/Ga_2O_3 superlattices coherently grown on r -plane sapphire. *Appl. Phys. Express.* **11**, 065501 (2018).
22. D. Shiojiri, R. Yamaguchi, S. Kaneko, A. Matsuda, M. Yoshimoto, Homoepitaxial growth of α-Al_2O_3 thin films on atomically stepped sapphire substrates by pulsed laser deposition at room-temperature. *J. Ceram. Soc. Japan.* **121**, 467–469 (2013).
23. M. Lorenz, S. Hohenberger, E. Rose, M. Grundmann, Atomically stepped, pseudomorphic, corundum-phase $(Al_{1-x}Ga_x)_2O_3$ thin films ($0 \leq x < 0.08$) grown on R-plane sapphire. *Appl. Phys. Lett.* **113**, 231902 (2018).
24. Y. Oshima, E. G. Víllora, K. Shimamura, Halide vapor phase epitaxy of twin-free α-Ga_2O_3 on sapphire (0001) substrates. *Appl. Phys. Express.* **8**, 055501 (2015).
25. D.-W. Jeon, H. Son, J. Hwang, A. Y. Polyakov, N. B. Smirnov, I. V. Shchemerov, A. V. Chernykh, A. I. Kochkova, S. J. Pearton, I.-H. Lee, Electrical properties, structural properties, and deep trap spectra of thin α-Ga_2O_3 films grown by halide vapor phase epitaxy on basal plane sapphire substrates. *APL Mater.* **6**, 121110 (2018).
26. R. Kumaran, T. Tiedje, S. E. Webster, S. Penson, W. Li, Epitaxial Nd-doped Nd-doped α-$(Al_{1-x}Ga_x)_2O_3$ films on sapphire for solid-state waveguide lasers. *Opt. Lett.* **35**, 3793 (2010).
27. H. Ito, K. Kaneko, S. Fujita, Growth and band gap control of corundum-structured α-$(AlGa)_2O_3$ thin films on sapphire by spray-assisted mist chemical vapor deposition. *Jpn. J. Appl. Phys.* **51**, 100207 (2012).
28. R. Jinno, T. Uchida, K. Kaneko, S. Fujita, Reduction in edge dislocation density in corundum-structured α-Ga_2O_3 layers on sapphire substrates with quasi-graded α-$(Al,Ga)_2O_3$ buffer layers. *Appl. Phys. Express* **9**, 59–62 (2016).
29. T. Uchida, R. Jinno, S. Takemoto, K. Kaneko, S. Fujita, Evaluation of band alignment of α-Ga_2O_3/α-$(Al_xGa_{1-x})_2O_3$ heterostructures by x-ray photoelectron spectroscopy. *Jpn. J. Appl. Phys.* **57**, 040314 (2018).
30. G. T. Dang, T. Yasuoka, Y. Tagashira, T. Tadokoro, W. Theiss, T. Kawaharamura, Bandgap engineering of α-$(Al_xGa_{1-x})_2O_3$ by a mist chemical vapor deposition two-chamber system and verification of Vegard's Law. *Appl. Phys. Lett.* **113**, 062102 (2018).
31. E. Ahmadi, O. S. Koksaldi, X. Zheng, T. Mates, Y. Oshima, U. K. Mishra, J. S. Speck, Modulation-doped β-$(Al_{0.2}Ga_{0.8})_2O_3$/Ga_2O_3 field-effect transistor. *Appl. Phys. Express.* **10**, 071101 (2017).
32. S. Krishnamoorthy, Z. Xia, C. Joishi, Y. Zhang, J. McGlone, J. Johnson, M. Brenner, A. R. Arehart, J. Hwang, S. Lodha, S. Rajan, Modulation-doped β-$(Al_{0.2}Ga_{0.8})_2O_3$/Ga_2O_3 field-effect transistor. *Appl. Phys. Lett.* **111**, 023502 (2017).
33. R. Schewski, G. Wagner, M. Baldini, D. Gogova, Z. Galazka, T. Schulz, T. Remmele, T. Markurt, H. von Wenckstern, M. Grundmann, O. Bierwagen, P. Vogt, M. Albrecht, Epitaxial stabilization of pseudomorphic α-Ga_2O_3 on sapphire (0001). *Appl. Phys. Express.* **8**, 011101 (2015).
34. Z. Cheng, M. Hanke, P. Vogt, O. Bierwagen, A. Trampert, Phase formation and strain relaxation of Ga_2O_3 on c-plane and a-plane sapphire substrates as studied by synchrotron-based x-ray diffraction. *Appl. Phys. Lett.* **111**, 162104 (2017).
35. F. Wang, J. Shan, E. Knoesel, M. Bonn, T. F. Heinz, in *Ultrafast Phenomena in Semiconductors and Nanostructure Materials VIII*, K.-T. Tsen, J.-J. Song, H. Jiang, Eds. (International Society for Optics and Photonics, 2004), vol. 5352, p. 216; https://doi.org/10.1117/12.532505.
36. S. Curiotto, D. Chatain, Surface morphology and composition of *c*-, *a*- and *m*-sapphire surfaces in O_2 and H_2 environments. *Surf. Sci.* **603**, 2688–2697 (2009).
37. H. Peelaers, J. B. Varley, J. S. Speck, C. G. Van de Walle, Structural and electronic properties of Ga_2O_3-Al_2O_3. *Appl. Phys. Lett.* **112**, 242101 (2018).
38. I. Vurgaftman, J. R. Meyer, L. R. Ram-Mohan, Band parameters for III-V compound semiconductor and their alloys. *J. Appl. Phys.* **89**, 11 (2001).
39. C. G. Dunn, E. F. Kogh, Comparison of dislocation densities of primary and secondary recrystallisation grains of Si–Fe. *Acta MetalI.* **5**, 548–554 (1957).
40. M. A. Moram, M. E. Vickers, X-ray diffraction of III-nitrides. *Rep. Prog. Phys.* **72**, 036502 (2009).
41. K. Kaneka, H. Kawanowa, H. Ito, S. Fujita, Evaluation of misfit relaxation in α-Ga_2O_3 epitaxial growth on α-Al_2O_3 substrate. *Jpn. J. Appl. Phys.* **51**, 0202201 (2012).

Acknowledgments: We acknowledge useful discussions with M. Thompson, F. Rana, J. McCandless, Y.-T. Shao, and N. Tanen of Cornell University and K. Chabak, A. Neal, A. Green, S. Mou, and T. Asel of the Air Force Research Laboratories. **Funding:** This work was, in part, supported by JSPS Overseas Challenge Program for Young Researchers 1080033 and by the Air-Force/Cornell Center for Epitaxial Solutions (ACCESS) center of excellence monitored by A. Sayir. C.S.C. acknowledges support from the Air Force Office of Scientific Research (FA9550-18-1-0529). **Author contributions:** R.J., Y.C., and D.J. conceived the study and designed the experimental study. R.J., C.S.C., T.O., S.-T.H., D.R., M.C.C., and K.L. performed the experiments. R.J., C.S.C., T.O., and Y.C. conducted the subsequent data analysis. R.J., C.S.C., and D.J. wrote the manuscript. V.P., D.G.S., D.A.M., and H.G.X. contributed ideas and feedback on the analysis and edited the manuscript. All authors edited the manuscript and approved its final version. **Competing interests:** The authors declare that they have no competing interests. **Data and materials availability:** All data needed to evaluate the conclusions in the paper are present in the paper and/or the Supplementary Materials. Additional data related to this paper may be requested from the authors.

Submitted 30 June 2020
Accepted 16 November 2020
Published 8 January 2021
10.1126/sciadv.abd5891

Citation: R. Jinno, C. S. Chang, T. Onuma, Y. Cho, S.-T. Ho, D. Rowe, M. C. Cao, K. Lee, V. Protasenko, D. G. Schlom, D. A. Muller, H. G. Xing, D. Jena, Crystal orientation dictated epitaxy of ultrawide-bandgap 5.4- to 8.6-eV α-$(AlGa)_2O_3$ on m-plane sapphire. *Sci. Adv.* **7**, eabd5891 (2021).

Downloaded from http://advances.sciencemag.org/ on January 12, 2021

ScienceAdvances

Crystal orientation dictated epitaxy of ultrawide-bandgap 5.4- to 8.6-eV α-$(AlGa)_2O_3$ on m-plane sapphire

Riena Jinno, Celesta S. Chang, Takeyoshi Onuma, Yongjin Cho, Shao-Ting Ho, Derek Rowe, Michael C. Cao, Kevin Lee, Vladimir Protasenko, Darrell G. Schlom, David A. Muller, Huili G. Xing and Debdeep Jena

Sci Adv **7** (2), eabd5891.
DOI: 10.1126/sciadv.abd5891

ARTICLE TOOLS http://advances.sciencemag.org/content/7/2/eabd5891

SUPPLEMENTARY MATERIALS http://advances.sciencemag.org/content/suppl/2021/01/04/7.2.eabd5891.DC1

REFERENCES This article cites 39 articles, 1 of which you can access for free
http://advances.sciencemag.org/content/7/2/eabd5891#BIBL

PERMISSIONS http://www.sciencemag.org/help/reprints-and-permissions

Use of this article is subject to the Terms of Service

Science Advances (ISSN 2375-2548) is published by the American Association for the Advancement of Science, 1200 New York Avenue NW, Washington, DC 20005. The title *Science Advances* is a registered trademark of AAAS.

Copyright © 2021 The Authors, some rights reserved; exclusive licensee American Association for the Advancement of Science. No claim to original U.S. Government Works. Distributed under a Creative Commons Attribution NonCommercial License 4.0 (CC BY-NC).

Downloaded from http://advances.sciencemag.org/ on January 12, 2021

Science Advances
AAAS

advances.sciencemag.org/cgi/content/full/7/2/eabd5891/DC1

Supplementary Materials for

Crystal orientation dictated epitaxy of ultrawide-bandgap 5.4- to 8.6-eV α-$(AlGa)_2O_3$ on m-plane sapphire

Riena Jinno, Celesta S. Chang, Takeyoshi Onuma, Yongjin Cho, Shao-Ting Ho, Derek Rowe, Michael C. Cao, Kevin Lee, Vladimir Protasenko, Darrell G. Schlom, David A. Muller, Huili G. Xing, Debdeep Jena*

*Corresponding author. Email: djena@cornell.edu

Published 8 January 2021, *Sci. Adv.* **7**, eabd5891 (2021)
DOI: 10.1126/sciadv.abd5891

This PDF file includes:

Supplementary Materials

Table S1. The Al and Ga BEPs and film thicknesses of the α-$(Al_xGa_{1-x})_2O_3$ films grown on *m*-plane sapphire substrates.

x	0	0.22	0.37	0.54	0.59	0.74	1
Al BEP (10^{-9} Torr)	0	1.5	4.9	9	9	9	16
Ga BEP (10^{-9} Torr)	9	7.5	9	9	4.7	3	0
Film thickness d (nm)	57	56	66	84.3	63.8	58.1	~60

Reciprocal Space Maps of α-Ga_2O_3 and α-$(Al_{0.18}Ga_{0.82})_2O_3$ on m-plane Sapphire Substrates

Asymmetric RSMs were measured for the α-Ga_2O_3 and α-$(Al_{0.18}Ga_{0.82})_2O_3$ epitaxial films grown on m-plane sapphire substrates. The growth conditions of the films are similar to what is discussed in the main text. The film thicknesses of the α-Ga_2O_3 and α-$(Al_{0.18}Ga_{0.82})_2O_3$ determined by XRR measurements were 52 and 57 nm. As shown in Fig. S1, both α-Ga_2O_3 and α-$(Al_{0.18}Ga_{0.82})_2O_3$ films, though single-crystalline, are lattice-relaxed due to the large lattice mismatch to the sapphire substrates. This is similar to the growth of GaN on SiC, Sapphire, or Silicon.

Symmetric XRD ω-Scan

The tilt in the MBE grown α-$(Al_xGa_{1-x})_2O_3$ films on m-plane sapphire substrates was estimated by performing symmetric ω-scan rocking curve measurements for the α-Ga_2O_3, α-$(Al_{0.18}Ga_{0.82})_2O_3$ films shown in Fig S1(a) and (b), and the α-$(Al_{0.54}Ga_{0.46})_2O_3$ film discussed in the main paper. The full-width at half maximum (FWHM) of the ω-scan (β) for x=0 is 0.58 degree (2088 arcsec) [Fig. S1(c)], a value close to α-Ga_2O_3 grown on m-plane sapphire by mist-CVD (*34*). The sample with the higher Al content shows a smaller FWHM of the ω-scan due to the smaller lattice mismatch between the film and the substrate [Fig. S1(c)]. The screw dislocation density (D_B) was estimated using the random distribution formula proposed by Dunn and Koch (*40*):

$$D_B = \frac{\beta^2}{9b^2}. \qquad (1)$$

Here, we have assumed the burgers vector (b) of $<10\bar{1}0>$. The estimated screw dislocation density is of the order ~10^{10} cm^{-2} for x=0, 0.18, 0.54 samples.

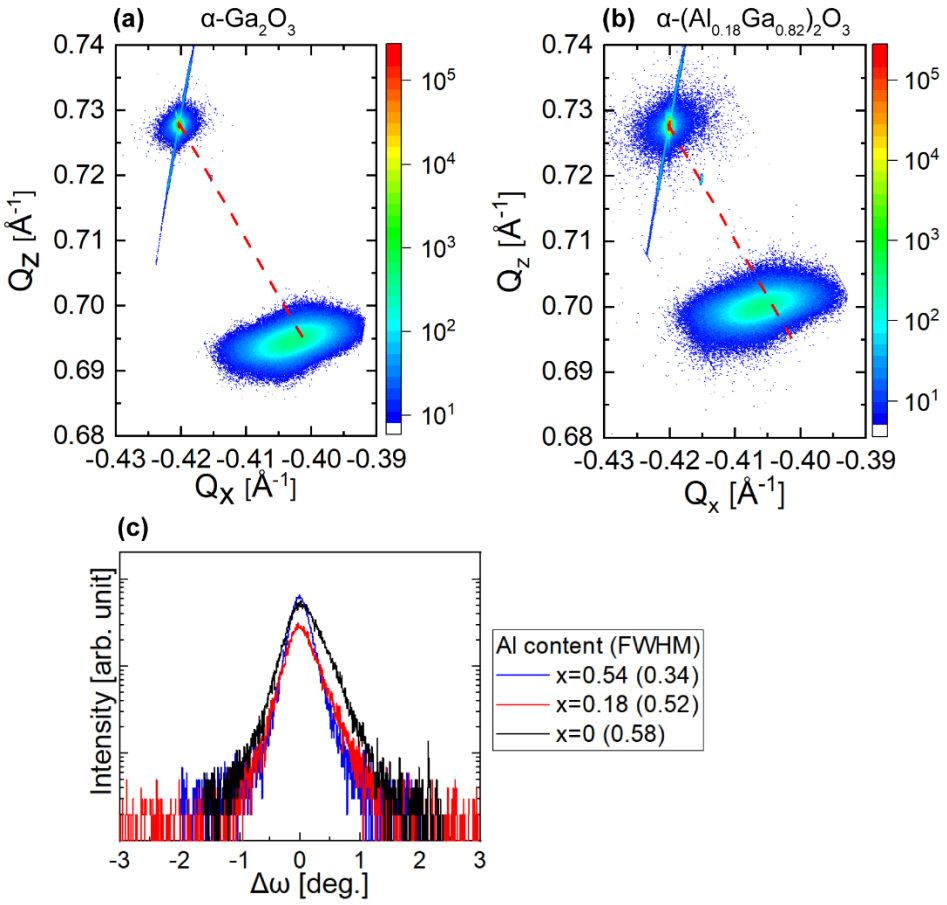

Fig. S1. Reciprocal space maps and symmetric rocking curves of the α-(Al_xGa_{1-x})$_2O_3$ films. Reciprocal space maps (Q_x, Q_z) around the $22\bar{4}0$ reflections of the (**a**) α-Ga_2O_3 and (**b**) α-($Al_{0.18}Ga_{0.82}$)$_2O_3$ epitaxial films. (**c**) Symmetric ($30\bar{3}0$) rocking curves of the α-(Al_xGa_{1-x})$_2O_3$ films with x= 0, 0.18 and 0.54.

XRD In-Plane Measurements and Skew-Symmetric ω-Scan

We measured the XRD in-plane $2\theta_\chi/\phi$ scans for α-(Al_xGa_{1-x})$_2O_3$ films with x= 0, 0.5 and 1 using Cu $K\bar{\alpha}$ ($K\alpha_1$+ $K\alpha_2$) radiation without a monochromator. The growth conditions of these samples are similar to what is described in the main text. The in-plane $2\theta_\chi/\phi$ scans can detect inclusions in thin films that are difficult to be observed in symmetric 2θ/ω scans (*12*). Figures S2(a) and (b) plot the measured XRD spectra for (0006) and ($11\bar{2}0$) planes of the α-(Al_xGa_{1-x})$_2O_3$ films, respectively. The diffraction peaks from the α-(Al_xGa_{1-x})$_2O_3$ 0006 and $11\bar{2}0$ shift to higher angle with increasing Al composition x. No peaks from other crystal phases or other planes are observed. The $2\theta_\chi/\phi$ scans for the α-(Al_xGa_{1-x})$_2O_3$ $11\bar{2}0$ detect diffraction peaks originating from Cu Kβ radiation since the incident x-ray was not monochromatic. The profile for the α-Ga_2O_3 film displays the peak from sapphire $11\bar{2}0$, but no intensity from sapphire 0006. On the other hand, the profiles for x=0.5 do not show diffraction peaks arising from sapphire substrates for both planes. This is because of the short penetration length of the x-ray of around 50 nm in the in-plane measurement, and it can also be attributed to the smaller intensity of the 0006 reflection than the $11\bar{2}0$ one.

To investigate tilt and twist values in the films, we also measured skew symmetric ω-scan profiles for the samples with x=0 and 0.5. The tilt and twist can be separated using the equation $\beta_{hkl}^2 = (\beta_{tilt}\cos\chi)^2 + (\beta_{twist}\sin\chi)^2$(*41*). Here, β_{hkl} is the ω-FWHM of the *hkl* reflection and this is

particularly useful for highly defective films. A series of skew symmetric ω-FWHM versus χ angle gives both tilt and twist. In this study, the ω-FWHM of the $30\bar{3}0$, $11\bar{2}0$, $03\bar{3}0$, and $10\bar{1}4$ reflections were used [Fig. S2(c) and (d)]. The ω-FWHM of the $10\bar{1}4$ reflection was obtained only for x=0 since the $10\bar{1}4$ reflections of α-$(Al_xGa_{1-x})_2O_3$ and sapphire are too close. The screw and edge dislocation densities were estimated using the Dunn and Koch formula of equation (1) by assuming the burgers vectors of <$11\bar{2}0$> and <0001>, as summarized in Table S2. The edge dislocation densities with b=<$11\bar{2}0$> and <0001> were on the order of 10^{11} and 10^9 cm^{-2}, respectively. The density with b=<$11\bar{2}0$> agree with that (~10^{11} cm^{-2}) obtained from TEM observation for Al composition of x=0.37. The edge dislocation with the burgers vector of <$11\bar{2}0$> was also dominant in the α-Ga_2O_3 film grown on c-plane sapphire by mist-CVD where a dislocation density of 7×10^{10} cm^{-2} was reported (*42*).

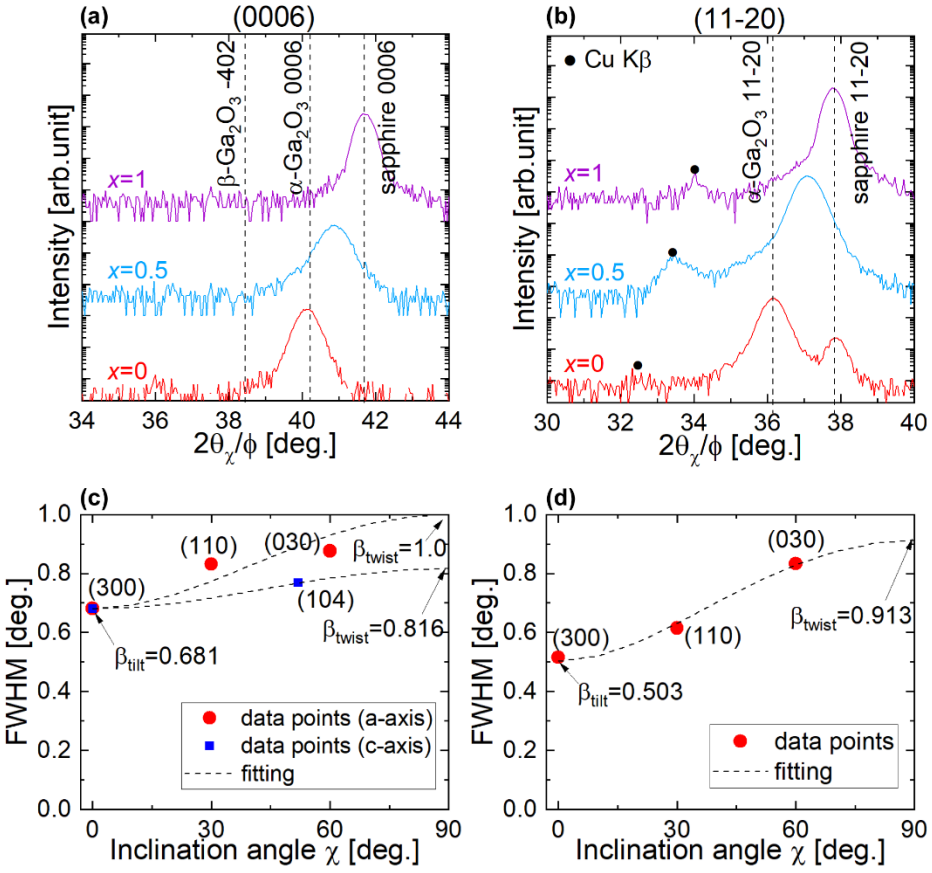

Fig. S2. XRD in-plane $2\theta_\chi/\phi$ scan profiles and ω-scan FWHM of the α-$(Al_xGa_{1-x})_2O_3$ films (x=0, 0.5). (a) 0006 and (b) $11\bar{2}0$ XRD in-plane $2\theta_\chi/\phi$ scan profiles of α-$(Al_xGa_{1-x})_2O_3$ films with x= 0, 0.5 and 1. The black dots in (b) denote the diffraction peaks originating from the Cu Kβ radiation. ω-scan FWHM taken from a series of reflections at increasing angle χ with respect to the $30\bar{3}0$ planes for the α-$(Al_xGa_{1-x})_2O_3$ films with (c) x= 0, and (d) x= 0.5.

Table S2. Summary of screw and edge dislocation density in the α-$(Al_xGa_{1-x})_2O_3$ films grown on m-plane sapphire substrates (x=0 and 0.5).

x	0	0.5
Screw	2.8×10^{10} cm^{-2}	2.3×10^{10} cm^{-2}
Edge <11$\bar{2}$0>	1.2×10^{11} cm^{-2}	1.3×10^{11} cm^{-2}
Edge <0001>	3.4×10^{9} cm^{-2}	

Observation of Defects in α-Ga_2O_3 by TEM Imaging

To further confirm that the samples grown are single phase, we performed selected area electron diffraction (SAED) imaging using FEI T-12 operating at 120 kV. Figure S3 shows an example of the epitaxial α-Ga_2O_3 sample. The electron diffraction pattern for the α-Ga_2O_3/m-plane sapphire shows two 'concentric' hexagonal patterns [Fig. S3(a)]. The lattice constant of sapphire is smaller than that of α-Ga_2O_3, resulting in the hexagonal diffraction pattern of the sapphire being slightly further from the center. In Fig. S3(b), the dark-field TEM image is color-coded in red and blue, where each color shows the signals coming from the inner α-Ga_2O_3 (circled in red) and outer sapphire diffraction spot (circled in blue) from Fig. S3(a). The α-Ga_2O_3 epitaxial layer is not completely red, because strain has distorted the lattice and therefore some regions in the film are not perfectly on the same crystal zone axis.

HAADF-STEM images at the α-Ga_2O_3/α-Al_2O_3 heterojunction show that the α-Ga_2O_3 layer is relaxed at the interface through the introduction of misfit dislocations [Fig. S3(c)]. In addition, some isolated areas near the substrate interface exhibit a crystal structure different from α-Ga_2O_3 [Fig. S3(d)]. In contrast to the α-Ga_2O_3 viewed down along <0001> zone axis, the defective region displays a distinctive pattern of edge-sharing rings. The schematic explains how such defective regions can form. When α-Ga_2O_3 is viewed along the <0001> zone axis, the Ga atoms arrange in a traditional hexagonal-closed-packed (hcp) structural form, as shown in the green atomic lattice structure. Here the following displacements occur: the yellow crystal structure, identical to the green, glides by two-thirds of the unit cell along the <11$\bar{2}$0> axis (horizontal direction). As HAADF-STEM images are obtained by averaging through several unit cells in projection, such a glide can result in the overlap seen in the lattice structure in the image resulting in the observed chained hexagonal lattice regions. This displacement is found to occur in different glide directions and distances as well, resulting in distinctive lattice structures in some isolated regions in the film. This stacking fault seems to originate at the interface, perhaps caused by the strain at the interface. In addition to α-Ga_2O_3, this defect was also observed in the low Al-content α-$(Al_{0.22}Ga_{0.78})_2O_3$ films. For α-$(Al_{0.37}Ga_{0.63})_2O_3$, we observed regions with poor lattice contrast inside the film, which we believe is potentially caused by defective regions including edge dislocations that jog along the projection direction. Although the dislocations and the stacking faults exist near at the heterointerface in the high Ga-content α-$(Al_xGa_{1-x})_2O_3$ layers, STEM images indicate single-crystalline, single phase epitaxial films are successfully grown on the m-plane sapphire substrate over the full $0\leq x\leq1$ composition range. No defects are observable in STEM in the α-Al_2O_3 epitaxial layer.

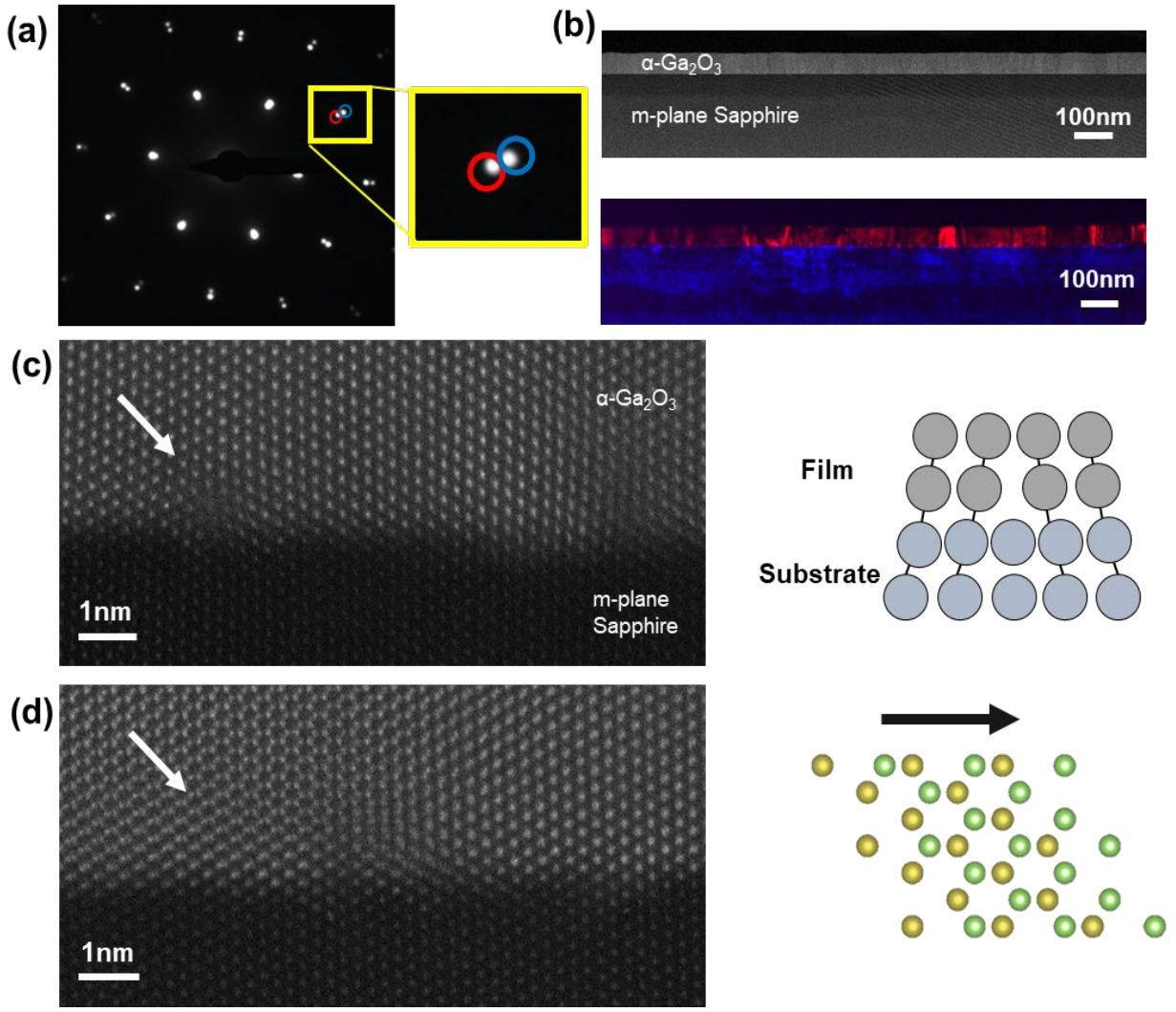

Fig. S3. Cross-sectional STEM images of the α-(Al_xGa_{1-x})$_2O_3$ film with x=0. (a) Diffraction yields two similar hexagonal patterns each originating from α-Ga_2O_3 and sapphire. As the lattice constant of sapphire is slightly smaller than that of α-Ga_2O_3, the outer diffraction spot of the two adjacent spots shown (circled in blue) corresponds to sapphire as shown in (b). The inner spot (circled in red) corresponds to the α-Ga_2O_3 film. False-color dark-field image overlay corresponding to each diffraction spots circled in blue and red are shown in (b), together with a HAADF-STEM image. The dark-field image of the α-Ga_2O_3 film is not completely color-coded in red as the strain has distorted the lattice. (c) Enlarged epitaxial interface reveals the atomic structure that is relaxing the strain. The schematic shows the corresponding edge dislocation. (d) Defective areas showing different hexagonal crystal structure from that of α-Ga_2O_3 that is caused by strain at the interface. A schematic of α-Ga_2O_3 crystal structure is also shown to explain how such hexagonal crystal lattices can form. When the yellow α-Ga_2O_3 crystal structure glides by two-thirds of the unit cell along the <11$\bar{2}$0> axis, the resulting crystal structure appears as a chained hexagonal structure when seen in projection in TEM.

REFERENCES AND NOTES

1. A. M. Armstrong, M. W. Moseley, A. A. Allerman, M. H. Crawford, J. J. Wierer, Growth temperature dependence of Si doping efficiency and compensating deep level defect incorporation in $Al_{0.7}Ga_{0.3}N$. *J. Appl. Phys.* **117**, 185704 (2015).

2. R. J. Kaplar, A. A. Allerman, A. M. Armstrong, M. H. Crawford, J. R. Dickerson, A. J. Fischer, A. G. Baca, E. A. Douglas, Review—Ultra-wide-bandgap AlGaN power electronic devices. *ECS J. Solid State Sci. Technol.* **6**, Q3061–Q3066 (2017).

3. S. Fujita, M. Oda, K. Kaneko, T. Hitora, Evolution of corundum-structured III-oxide semiconductors: Growth, properties, and devices. *Jpn. J. Appl. Phys.* **55**, 1202A3 (2016).

4. J. Y. Tsao, S. Chowdhury, M. A. Hollis, D. Jena, N. M. Johnson, K. A. Jones, R. J. Kaplar, S. Rajan, C. G. Van de Walle, E. Bellotti, C. L. Chua, R. Collazo, M. E. Coltrin, J. A. Cooper, K. R. Evans, S. Graham, T. A. Grotjohn, E. R. Heller, M. Higashiwaki, M. S. Islam, P. W. Juodawlkis, M. A. Khan, A. D. Koehler, J. H. Leach, U. K. Mishra, R. J. Nemanich, R. C. N. Pilawa-Podgurski, J. B. Shealy, Z. Sitar, M. J. Tadjer, A. F. Witulski, M. Wraback, J. A. Simmons, Ultrawide-bandgap semiconductors: Research opportunities and challenges. *Adv. Electron. Mater.* **4**, 1600501 (2018).

5. M. Higashiwaki, K. Sasaki, A. Kuramata, T. Masui, S. Yamakoshi, Gallium oxide (Ga_2O_3) metal-semiconductor field-effect transistors on single-crystal β-Ga_2O_3 (010) substrates. *Appl. Phys. Lett.* **100**, 013504 (2012).

6. W. Li, K. Nomoto, Z. Hu, T. Nakamura, D. Jena, H. G. Xing, in *2019 IEEE International Electron Devices Meeting (IEDM)* (IEEE, 2019), pp. 12.4.1–12.4.4; https://ieeexplore.ieee.org/document/8993526/.

7. T. Oshima, T. Okuno, N. Arai, Y. Kobayashi, S. Fujita, β-$Al_{2x}Ga_{2-2x}O_3$ thin film growth by molecular beam epitaxy. *Jpn. J. Appl. Phys.* **48**, 070202 (2009).

8. S. W. Kaun, F. Wu, J. S. Speck, β-$(Al_xGa_{1-x})_2O_3/Ga_2O_3$ (010) heterostructures grown on β-Ga_2O_3 (010) substrates by plasma-assisted molecular beam epitaxy. *J. Vac. Sci. Technol.* **33**, 041508 (2015).

9. A. F. M. Anhar Uddin Bhuiyan, Z. Feng, J. M. Johnson, Z. Chen, H.-L. Huang, J. Hwang, H. Zhao, MOCVD epitaxy of β-$(Al_xGa_{1-x})_2O_3$ thin films on (010) Ga_2O_3 substrates and N-type doping. *Appl. Phys. Lett.* **115**, 120602 (2019).

10. A. F. M. A. U. Bhuiyan, Z. Feng, J. M. Johnson, H.-L. Huang, J. Sarker, M. Zhu, M. R. Karim, B. Mazumder, J. Hwang, H. Zhao, Phase transformation in MOCVD growth of $(Al_xGa_{1-x})_2O_3$ thin films. *APL Mater.* **8**, 031104 (2020).

11. R. H. French, Electronic band structure of Al_2O_3, with comparison to Alon and AIN. *J. Am. Ceram. Soc.* **73**, 477–489 (1990).

12. D. Shinohara, S. Fujita, Heteroepitaxy of corundum-structured α-Ga_2O_3 thin films on α-Al_2O_3 substrates by ultrasonic mist chemical vapor deposition. *Jpn. J. Appl. Phys.* **47**, 7311–7313 (2008).

13. A. Segura, L. Artús, R. Cuscó, R. Goldhahn, M. Feneberg, Band gap of corundumlike α–Ga_2O_3 determined by absorption and ellipsometry. *Phys. Rev. Mater.* **1**, 024604 (2017).

14. M. Kracht, A. Karg, M. Feneberg, J. Bläsing, J. Schörmann, R. Goldhahn, M. Eickhoff, Anisotropic optical properties of metastable $(01\bar{1}2)$ α-Ga_2O_3 grown by plasma-assited molecular beam epitaxy. *Phys. Rev. Appl.* **10**, 024047 (2018).

15. A. K. Harman, S. Ninomiya, S. Adachi, Optical constants of sapphire (α-Al_2O_3) single crystals. *J. Appl. Phys.* **76**, 8032–8036 (1994).

16. J. Fontanella, C. Andeen, D. Schuele, Low-frequency dielectric constants of α-quartz, sapphire, MgF_2, and MgO. *J. Appl. Phys.* **45**, 2852–2854 (1974).

17. K. Akaiwa, S. Fujita, Electrical conductive corundum-structured α-Ga_2O_3 thin films on sapphire with tin-doping grown by spray-assisted mist chemical vapor deposition. *Jpn. J. Appl. Phys.* **51**, 070203 (2012).

18. K. Akaiwa, K. Ota, T. Sekiyama, T. Abe, T. Shinohe, K. Ichino, Electrical properties of Sn-doped α-Ga_2O_3 films on m-plane sapphire substrates grown by mist chemical vapor deposition. *Phys. status solidi.* **217**, 1900632 (2020).

19. J. B. Varley, A. Perron, V. Lordi, D. Wickramaratne, J. L. Lyons, Prospects for n -type doping of $(Al_xGa_{1-x})_2O_3$ alloys. *Appl. Phys. Lett.* **116**, 172104 (2020).

20. T. Maeda, M. Yoshimoto, T. Ohnishi, G. H. Lee, H. Koinuma, Orientation-defined molecular layer epitaxy of α-Al_2O_3 thin films. *J. Cryst. Growth* **177**, 95–101 (1997).

21. T. Oshima, Y. Kato, M. Imura, Y. Nakayama, M. Takeguchi, α-Al_2O_3/Ga_2O_3 superlattices coherently grown on r -plane sapphire. *Appl. Phys. Express.* **11**, 065501 (2018).

22. D. Shiojiri, R. Yamaguchi, S. Kaneko, A. Matsuda, M. Yoshimoto, Homoepitaxial growth of α-Al_2O_3 thin films on atomically stepped sapphire substrates by pulsed laser deposition at room-temperature. *J. Ceram. Soc. Japan.* **121**, 467–469 (2013).

23. M. Lorenz, S. Hohenberger, E. Rose, M. Grundmann, Atomically stepped, pseudomorphic, corundum-phase $(Al_{1-x}Ga_x)_2O_3$ thin films ($0 \leq x < 0.08$) grown on R-plane sapphire. *Appl. Phys. Lett.* **113**, 231902 (2018).

24. Y. Oshima, E. G. Víllora, K. Shimamura, Halide vapor phase epitaxy of twin-free α-Ga_2O_3 on sapphire (0001) substrates. *Appl. Phys. Express.* **8**, 055501 (2015).

25. D.-W. Jeon, H. Son, J. Hwang, A. Y. Polyakov, N. B. Smirnov, I. V. Shchemerov, A. V. Chernykh, A. I. Kochkova, S. J. Pearton, I.-H. Lee, Electrical properties, structural properties, and deep trap spectra of thin α-Ga_2O_3 films grown by halide vapor phase epitaxy on basal plane sapphire substrates. *APL Mater.* **6**, 121110 (2018).

26. R. Kumaran, T. Tiedje, S. E. Webster, S. Penson, W. Li, Epitaxial Nd-doped Nd-doped α-$(Al_{1-x}Ga_x)_2O_3$ films on sapphire for solid-state waveguide lasers. *Opt. Lett.* **35**, 3793 (2010).

27. H. Ito, K. Kaneko, S. Fujita, Growth and band gap control of corundum-structured α-$(AlGa)_2O_3$ thin films on sapphire by spray-assisted mist chemical vapor deposition. *Jpn. J. Appl. Phys.* **51**, 100207 (2012).

28. R. Jinno, T. Uchida, K. Kaneko, S. Fujita, Reduction in edge dislocation density in corundum-structured α-Ga_2O_3 layers on sapphire substrates with quasi-graded α-$(Al,Ga)_2O_3$ buffer layers. *Appl. Phys. Express*, **9**, 59–62 (2016).

29. T. Uchida, R. Jinno, S. Takemoto, K. Kaneko, S. Fujita, Evaluation of band alignment of α-Ga_2O_3/α-$(Al_xGa_{1-x})_2O_3$ heterostructures by x-ray photoelectron spectroscopy. *Jpn. J. Appl. Phys.* **57**, 040314 (2018).

30. G. T. Dang, T. Yasuoka, Y. Tagashira, T. Tadokoro, W. Theiss, T. Kawaharamura, Bandgap engineering of α-$(Al_xGa_{1-x})_2O_3$ by a mist chemical vapor deposition two-chamber system and verification of Vegard's Law. *Appl. Phys. Lett.* **113**, 062102 (2018).

31. E. Ahmadi, O. S. Koksaldi, X. Zheng, T. Mates, Y. Oshima, U. K. Mishra, J. S. Speck, Modulation-doped β-$(Al_{0.2}Ga_{0.8})_2O_3$/Ga_2O_3 field-effect transistor. *Appl. Phys. Express.* **10**, 071101 (2017).

32. S. Krishnamoorthy, Z. Xia, C. Joishi, Y. Zhang, J. McGlone, J. Johnson, M. Brenner, A. R. Arehart, J. Hwang, S. Lodha, S. Rajan, Modulation-doped β-$(Al_{0.2}Ga_{0.8})_2O_3$/Ga_2O_3 field-effect transistor. *Appl. Phys. Lett.* **111**, 023502 (2017).

33. R. Schewski, G. Wagner, M. Baldini, D. Gogova, Z. Galazka, T. Schulz, T. Remmele, T. Markurt, H. von Wenckstern, M. Grundmann, O. Bierwagen, P. Vogt, M. Albrecht, Epitaxial stabilization of pseudomorphic α-Ga_2O_3 on sapphire (0001). *Appl. Phys. Express.* **8**, 011101 (2015).

34. Z. Cheng, M. Hanke, P. Vogt, O. Bierwagen, A. Trampert, Phase formation and strain relaxation of Ga_2O_3 on c-plane and a-plane sapphire substrates as studied by synchrotron-based x-ray diffraction. *Appl. Phys. Lett.* **111**, 162104 (2017).

35. F. Wang, J. Shan, E. Knoesel, M. Bonn, T. F. Heinz, in *Ultrafast Phenomena in Semiconductors and Nanostructure Materials VIII*, K.-T. Tsen, J.-J. Song, H. Jiang, Eds. (2004), vol. 5352, p. 216; https://doi.org/10.1117/12.532505.

36. S. Curiotto, D. Chatain, Surface morphology and composition of *c*-, *a*- and *m*-sapphire surfaces in O_2 and H_2 environments. *Surf. Sci.* **603**, 2688–2697 (2009).

37. H. Peelaers, J. B. Varley, J. S. Speck, C. G. Van de Walle, Structural and electronic properties of Ga_2O_3-Al_2O_3. *Appl. Phys. Lett.* **112**, 242101 (2018).

38. I. Vurgaftman, J. R. Meyer, L. R. Ram-Mohan, Band parameters for III-V compound semiconductor and their alloys. *J. Appl. Phys.* **89**, 11 (2001).

39. C. G. Dunn, E. F. Kogh, Comparison of dislocation densities of primary and secondary recrystallisation grains of Si–Fe *Acta Metall.* **5** 548–554 (1957).

40. M. A. Moram, M. E. Vickers, X-ray diffraction of III-nitrides. *Rep. Prog. Phys.* **72**, 036502 (2009).

41. K. Kaneka, H. Kawanowa, H. Ito, S. Fujita, Evaluation of misfit relaxation in α-Ga_2O_3 epitaxial growth on α-Al_2O_3 substrate. *Jpn. J. Appl. Phys.* **51**, 0202201 (2012).